

On the Optical Properties of Thin-Film Vanadium Dioxide from the Visible to the Far Infrared

Chenghao Wan, Zhen Zhang, David Woolf, Colin M. Hessel, Jura Rensberg, Joel M. Hensley, Yuzhe Xiao, Alireza Shahsafi, Jad Salman, Steffen Richter, Yifei Sun, M. Mumtaz Qazilbash, Rüdiger Schmidt-Grund, Carsten Ronning, Shriram Ramanathan, and Mikhail A. Kats*

The insulator-to-metal transition (IMT) in vanadium dioxide (VO_2) can enable a variety of optics applications, including switching and modulation, optical limiting, and tuning of optical resonators. Despite the widespread interest in VO_2 for optics, the wavelength-dependent optical properties across its IMT are scattered throughout the literature, are sometimes contradictory, and are not available at all in some wavelength regions. Here, the complex refractive index of VO_2 thin films across the IMT is characterized for free-space wavelengths from 300 nm to 30 μm , using broadband spectroscopic ellipsometry, reflection spectroscopy, and the application of effective-medium theory. VO_2 films of different thicknesses are studied, on two different substrates (silicon and sapphire), and grown using different synthesis methods (sputtering and sol-gel). While there are differences in the optical properties of VO_2 synthesized under different conditions, these differences are surprisingly small in the $\approx 2\text{--}11\ \mu\text{m}$ range where the insulating phase of VO_2 also has relatively low optical loss. It is anticipated that the refractive-index datasets from this article will be broadly useful for modeling and design of VO_2 -based optical and optoelectronic components, especially in the mid-wave and long-wave infrared.

1. Introduction

Vanadium dioxide (VO_2) undergoes a first-order insulator-to-metal transition (IMT) at $\approx 68\ ^\circ\text{C}$, which can be driven thermally,^[1] electrically,^[2] optically,^[3] or via strain.^[4] This reversible phase transition is the result of an interplay between Mott- and Peierls-type mechanisms,^[5] and can result in carrier-density changes of up to four orders of magnitude across the IMT.^[6] The dramatic change in optical properties of VO_2 that accompanies the carrier-density change^[7] has advanced a variety of applications, including optical limiting,^[8,9] nonlinear isolation,^[10] switching,^[11,12] and thermal-emission engineering.^[13] Depending on the VO_2 film quality, grain size, the concentration and type of potential impurities, and the degree of strain, the phase transition can vary from abrupt to gradual.^[14–16] Either of these may

C. Wan, Dr. Y. Xiao, A. Shahsafi, J. Salman, Prof. M. A. Kats
Department of Electrical and Computer Engineering
University of Wisconsin–Madison
1415 Engineering Drive, Madison, WI 53705, USA
E-mail: mkats@wisc.edu

C. Wan, Prof. M. A. Kats
Department of Materials Science & Engineering
University of Wisconsin–Madison
Madison, WI 53706, USA

Dr. Z. Zhang, Dr. Y. Sun, Prof. S. Ramanathan
School of Materials Engineering
Purdue University
West Lafayette, IN 47907, USA

Dr. D. Woolf, Dr. C. M. Hessel, Dr. J. M. Hensley
Physical Sciences Inc.
20 New England Business Center
Andover, MA 01810-1077, USA


Dr. J. Rensberg, Prof. C. Ronning
Institute for Solid State Physics
Friedrich-Schiller-Universität Jena
07743 Jena, Germany

Dr. S. Richter, Dr. R. Schmidt-Grund
Felix Bloch Institute for Solid State Physics
Universität Leipzig
Linnéstr. 5, 04103 Leipzig, Germany

Dr. S. Richter
ELI Beamlines/Fyzikální ústav AV ČR, v.v.i.
Za Radnicí 835, 25241 Dolní Břežany, Czech Republic

Prof. M. M. Qazilbash
Department of Physics
College of William and Mary
Williamsburg, VA 23187-8795, USA

Dr. R. Schmidt-Grund
Institut für Physik
Technische Universität Ilmenau
Weimarer Straße 32, 98693 Ilmenau, Germany

 The ORCID identification number(s) for the author(s) of this article can be found under <https://doi.org/10.1002/andp.201900188>

DOI: 10.1002/andp.201900188

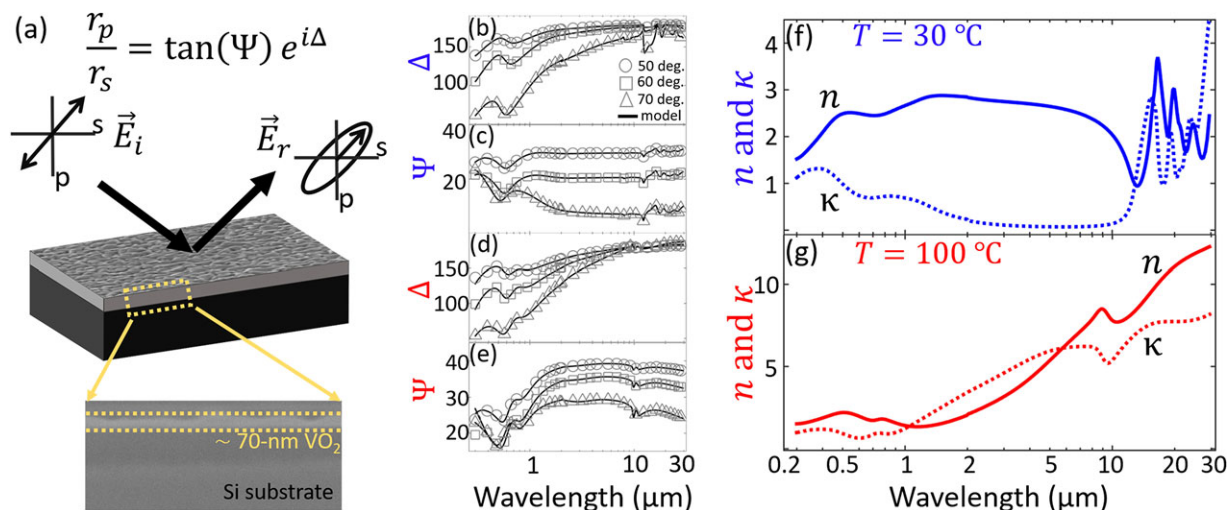


Figure 1. a) Schematic of our ellipsometry measurement, including the definitions of the ellipsometric measured data, Ψ and Δ . The inset is an SEM cross section of Film 1. The experimental (discrete points) and fitted (solid curves) Ψ and Δ for the b,c) insulating (30 °C) and d,e) metallic phase (100 °C) of Film 1. f,g) Extracted real (n) and imaginary (κ) parts of the complex refractive indices of Film 1 in its insulating and metallic phase, respectively, where our fitting process assumed no surface roughness, silicon-oxide layer on the silicon substrate, or potential non-stoichiometric contributions from other vanadium oxides.

be preferred depending on the application, for example abrupt transitions for switching^[12] and gradual transitions for tuning of optical resonances.^[17]

Knowledge of the complex refractive index of VO₂ across its IMT can enable computational design of various optical and optoelectronic devices incorporating this material. There is a large literature base of experiments that have been used to extract such optical properties; however, many of these investigations focus almost entirely on the visible and near-infrared ranges,^[7,18–21] with one recent study extending into the mid infrared.^[22]

The goal of this paper is to provide a comprehensive study of the optical properties of thin-film VO₂ across its IMT for free-space wavelengths from 300 nm to 30 μm, and to identify the wavelengths in which VO₂ is maximally useful as a tunable optical material. We studied films of different thickness (from ~70 to ~130 nm), grown by different methods (magnetron sputtering and sol-gel synthesis), and on different substrates (silicon and sapphire). To extract the complex refractive-index data, we used variable-angle spectroscopic ellipsometry (VASE),^[23] and verified the results with a combination of standard material-characterization techniques and non-ellipsometric optical measurements. To model the optical properties throughout the IMT, we used an effective-medium theory, which explains most of our experimental observations. Taken together, the results of this article can be used to perform optical simulations of VO₂-containing devices over the broadband range covering the ultraviolet to the far infrared, for VO₂ in the insulating and metallic phases, as well as in the intermediate regime throughout the IMT.

2. Experimental Section

For every VO₂ film that we studied, we performed two sets of VASE measurements: the first at shorter wavelengths (300 nm to 2.1 μm, using the V-VASE instrument from J. A. Woollam Co.), and the second at longer wavelengths (2 μm to 30 μm, IR-

VASE from J. A. Woollam Co.) (**Figure 1**). Both sets of measurements were performed at three incident angles of 50°, 60°, and 70°. Prior to the measurements, the back surfaces of the substrates were sandblasted to minimize backside reflections. The ellipsometry was carried out at two temperatures: 30 °C (VO₂ in the insulating phase) and 100 °C (in the metallic phase). For intermediate temperatures, we combined the ellipsometry data with temperature-dependent reflection measurements and calculated the temperature-dependent effective refractive index using an effective-medium theory (see next section). We chose this approach because ellipsometry at many temperatures throughout the IMT can result in artifacts due to temperature fluctuations combined with the hysteretic nature of the IMT; these artifacts are worse for ellipsometry than the reflectivity measurements because of the longer duration of a single ellipsometry measurements at a given temperature. The reflectance measurements were performed at near-normal incidence, for wavelengths from 2 μm to 17 μm, using an infrared microscope (Bruker Hyperion 2000) attached to a Fourier-transform infrared spectrometer (Bruker Vertex 70). All reflectance spectra were collected at temperatures between 30 and 100 °C (first heating, then cooling) with steps of 2 °C, and were normalized to a gold mirror, assuming a known reflectance of optically thick gold.

We selected four VO₂ thin-film samples with varying thickness, substrate, and synthesis method (**Table 1**); the synthesis details are in Section S1, Supporting Information. These

Table 1. List of samples characterized in this work.

	Thickness [nm]	Substrate	Synthesis method
Film 1	70 ± 9	Si + native oxide	Magnetron sputtering
Film 2	130 ± 17	Si + native oxide	Magnetron sputtering
Film 3	120 ± 12	Sapphire	Magnetron sputtering
Film 4	110 ± 5	Si + native oxide	Sol-gel

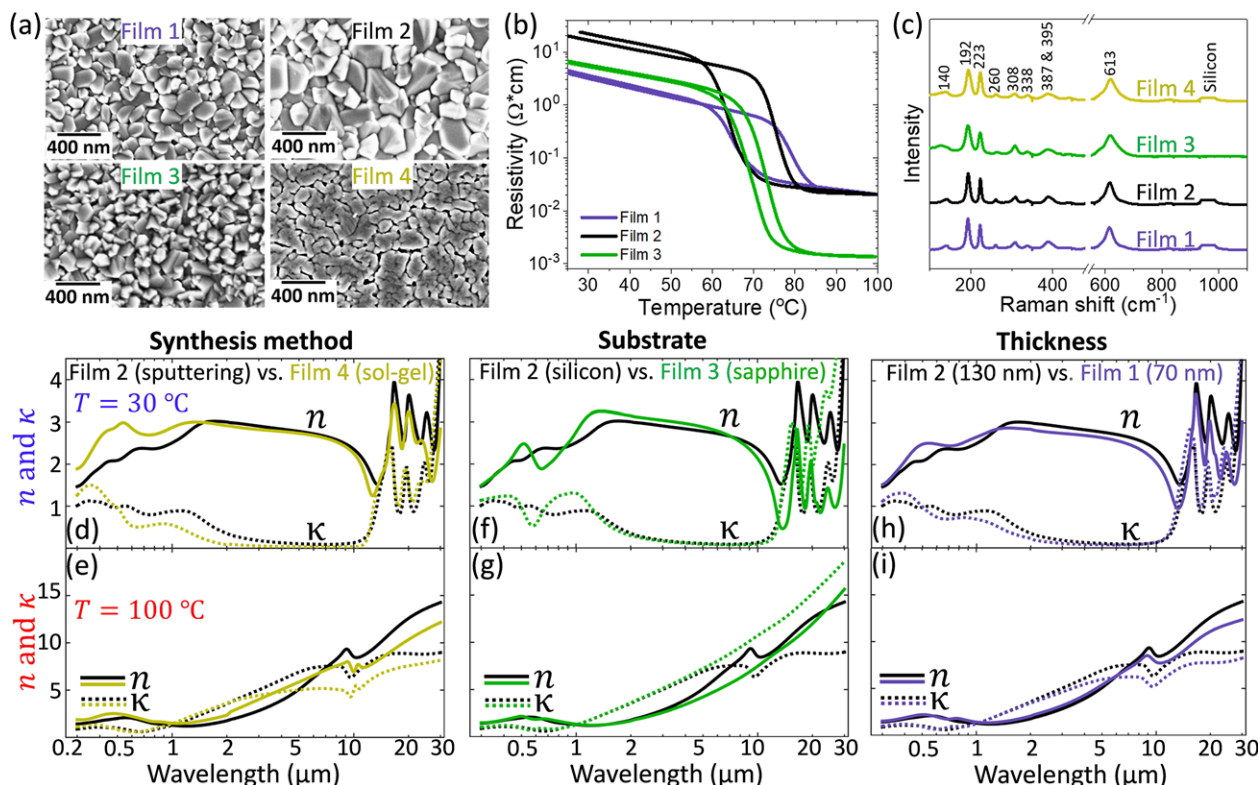


Figure 2. a) SEM images of the top surfaces of the four films described in this paper. b) Temperature-dependent measurements of resistivity across the IMT for Films 1–3. Samples were thermally driven via a cycle of heating and cooling. c) Room-temperature Raman spectra of Films 1–4. Note that there is a break in the x-axis from 480 to 550 cm^{-1} to exclude a strong peak due to silicon at $\approx 520 \text{ cm}^{-1}$. Bottom figures are pairs of comparison of the extracted refractive indices of the VO_2 films in Table 1 in the insulating (top) and metallic (bottom) phase, by different: d,e) synthesis methods; f,g) substrates; and h,i) film thicknesses. Note that the comparisons are between the four films in Table 1 and panel (a), and the results should not be interpreted as definitive for, for example, differences between all sputtered and sol-gel-synthesized VO_2 films.

samples were chosen such that there were three pairs that primarily differ in only one way for each pair: Films 1 and 2 grown using the same technique and on the same substrate, but with substantially different thickness (highlighted in purple), Films 2 and 3 grown to a similar thickness but on different substrates (highlighted in green), and Films 2 and 4 grown to a similar thickness on the same substrate but using different synthesis techniques (highlighted in yellow). The thicknesses given in Table 1 were measured using cross-sectional scanning electron microscopy (SEM), and the uncertainties are surface-roughness values determined using atomic force microscopy (AFM), as shown in Section S2, Supporting Information.

The thickness of the VO_2 film may affect its optical properties due to strain relaxation (the strain-relaxation thickness is in the tens of nanometers^[24,25]). To investigate this difference, we prepared VO_2 films on silicon (001) substrates (with a native oxide layer) with thickness of ≈ 70 and $\approx 130 \text{ nm}$ (Films 1 and 2) using the same magnetron-sputtering recipe.

Commonly, both silicon (001) and c -plane-oriented sapphire are used as substrates for VO_2 growth.^[26] The substrate choice can significantly affect the film quality, in part due to the lattice mismatch at the substrate-film interface.^[15,26] To explore the role of the substrate on the optical properties, we prepared sputtered films of similar thickness (≈ 120 and $\approx 130 \text{ nm}$), but on different substrates: silicon (001) with

a native oxide layer (Film 2), and c -plane-oriented sapphire (Film 3).

Finally, the growth technique can also have a large influence on the properties of VO_2 .^[27] Many synthesis techniques have been used for VO_2 growth, including sputtering,^[26] sol-gel synthesis,^[28] atomic-layer deposition,^[29] chemical-vapor deposition,^[30] and pulsed-laser deposition.^[31] Here, we compare films grown to a similar thickness (≈ 110 and $\approx 130 \text{ nm}$) on the same substrate (silicon with a native oxide layer), using magnetron sputtering (Film 2) and the sol-gel method (Film 4).

We imaged our samples with a scanning electron microscope (SEM, Zeiss LEO 1530) to confirm the continuity and uniformity of the films (Figure 2a). The magnetron-sputtered VO_2 films (Films 1, 2, and 3) feature similar multi-domain continuous morphology. Our sol-gel VO_2 film (Film 4) has less continuity (and, likely, slightly lower density) due to some small-scale cracks between domains. Post-growth temperature-dependent electrical resistance measurements (Figure 2b) were performed on the sputtered films on a temperature-controlled probe station. The resistance was obtained by measuring current while sweeping the voltage from -0.1 to 0.1 V , using a Keithley 2635A source meter. Film 3 features the largest change in resistivity across the IMT, indicating that it has the best film quality, likely due to the smaller lattice mismatch at the interface between VO_2 and c -plane-oriented sapphire. For Film 4, we were not able to see

the change in resistance across the IMT between two ≈ 5 -mm-separated electrodes, and the measured resistance is higher than that of the other films by several orders of magnitudes, so the data for this film is not shown. This large resistance in Film 4 is likely due to the discontinuities (small-scale cracks) in the film, as shown in Figure 2a. Further discussion can be found in Section 3.

We performed room-temperature Raman-spectroscopy measurements (LabRAM ARAMIS, Horiba) of the four films, with the pump laser operating at 520 nm (Figure 2c). All four films feature signature Raman modes of VO₂ at 140, 192, 223, 260, 308, 338, 387, 395, and 613 cm⁻¹, and we did not find any obvious features corresponding to other vanadium oxides, for example, at 284, 405, and 996 cm⁻¹ for V₂O₅.^[32] The plateaus between 950 and 1000 cm⁻¹ in Films 1, 2, and 4 are from the silicon substrates.^[32]

3. Data Analysis and Discussion

Our fitting procedure comprised the following basic steps. First, we fit the shorter-wavelength (300 nm to 2.1 μ m) data, obtaining the complex refractive index and the fitted thickness of the VO₂ film. The shorter-wavelength fit was carried out before moving to longer wavelengths because, for deeply subwavelength films, there may be no unique fit for both the thickness and complex refractive index.^[33,34] Therefore, it is advantageous to first fit at only the shorter wavelengths. Then, we used the thickness from the shorter-wavelength fit as an input parameter into the fitting model for the longer-wavelength fit (2–30 μ m). Finally, we confirmed that the resulting complex refractive index matched well between the two datasets in the spectral range where the two overlap, and that the fitted thickness matched the SEM/AFM measurements. We performed complete analysis of all of the films listed in Table 1, but for brevity only present all of the ellipsometric data for Film 1 in the main text (see Section S3, Supporting Information for the remaining data).

The experimental ellipsometric data (Ψ and Δ in Figure 1a) are shown in Figure 1b–e for Film 1 in both the insulating (30 °C) and metallic (100 °C) phase, obtained using the V-VASE and IR-VASE instruments. We performed shorter-wavelength fits from the V-VASE data first. Our fitting model consisted of a semi-infinite silicon substrate and the VO₂ film. The optical constants of the silicon substrate were taken from ref. [35], and the native oxide layer (thickness ≈ 3 nm) of silicon was neglected in the fitting, because it had little noticeable impact on the resulting fits (Section S3, Supporting Information). The thickness of the VO₂ layers was a fitting parameter for the insulating-phase VO₂, and we assumed that the thickness change during the transition (expected to be $\approx 0.6\%$ ^[36,37]) was smaller than our thickness uncertainty. We parametrized the model dielectric function for the VO₂ layer using a series of Lorentz oscillators^[23,38] for the insulating phase, and an additional Drude term to capture the contribution of the free carriers^[23,39] for the metallic phase. The parameters of these oscillator terms were fitted. We ignored the presence of surface roughness (arithmetic average roughness $R_a \approx 9$ nm based on AFM imaging), which is much smaller than the measurement wavelength. For the analysis that explicitly considers the surface roughness, see Section S3, Supporting Information.

The fitted thickness of VO₂ (≈ 69 nm) agrees with the cross-sectional SEM imaging to within the surface roughness (≈ 9 nm, by AFM, see Section S2, Supporting Information). This enabled us to initialize our long-wavelength fit (to the IR-VASE data) with a fixed effective optical thickness and no surface roughness layer. The resulting fit yielded the real (n) and imaginary (κ) parts of the complex refractive index throughout the mid- and far-infrared regions.

We plotted the full-spectrum complex refractive indices of Film 1 in both the insulating and metallic phases (Figure 1f,g) at 30 and 100 °C, respectively. The transition between the spectral regions of the two ellipsometers ($\lambda \approx 2$ μ m) is hardly noticeable in the data, indicating good agreement between these two separately fitted results. To further confirm the extracted complex refractive indices, we calculated the normal-incidence reflectance of this sample using the transfer-matrix method, which agrees well with FTIR reflectance measurements for both VO₂ phases (see Figure 4 and the corresponding text below).

We applied this characterization procedure to the other three samples, to compare the optical properties of VO₂ films for different synthesis methods (Figure 2d,e), substrates (Figure 2f,g), and thicknesses (Figure 2h,i). We note that for Film 3, grown on *c*-plane-oriented sapphire, our fitting procedure differs slightly from the one used for all of the other films due to the anisotropy and significant dispersion of sapphire in the mid- and far infrared. Details of the modified fitting procedure are discussed in Section S3, Supporting Information.

It is instructive to examine the differences and similarities between the optical properties of these four films, focusing on different wavelength ranges. For wavelengths below ≈ 2 μ m, which approximately corresponds to the energy region of interband transitions of VO₂ in its insulating phase (>0.6 eV^[40]), all of our films show substantial differences in their insulating-phase optical properties. Such large differences of optical properties in the visible and near-infrared ranges are also regularly found in the literature for different VO₂ samples^[7,18,19,22,41–44] (Figure 3). The band structure of the insulating state can be sensitive to a variety of factors, including strain, stoichiometry, grain size, and defects.^[15,26] All of these factors change with varying growth conditions,^[27] lattice matching to the substrate,^[15] and film thickness (and the resulting strain relaxation).^[25,45] The short-wavelength differences may also be in part due to the significant differences in the surface roughness, as seen by our SEM and AFM analysis (Section S2, Supporting Information). As discussed in Section S3, Supporting Information, there were slight changes in n and κ when we considered surface roughness in our ellipsometry modeling.

In the longest-wavelength region accessible to our measurements (11–30 μ m), insulating-phase VO₂ films feature three strong vibrational resonances (at approximately $\lambda = 17$, 20, and 25 μ m^[46]). In our measurements, these long-wavelength features do not appear to vary very much for different synthesis techniques (Figure 2d), do vary somewhat for different thickness (Figure 2h), and are quite distinct for different substrates (Figure 2f), probably due to different strain resulting from the lattice mismatch with the substrate. VO₂ crystal orientation, which varies significantly for films on different substrates, can also affect such phonon features.^[47] In the metallic phase, vibrational resonances are not observed, as the Drude contribution

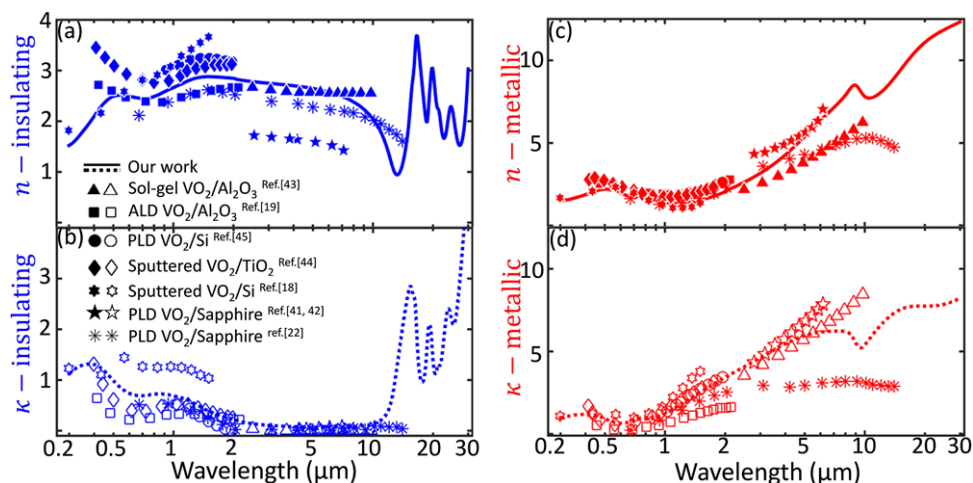


Figure 3. Comparison between the measured complex refractive index of Film 1 and some representative published data: a,b) real and imaginary parts of the refractive index of insulator-phase thin-film VO₂; c,d) real and imaginary part of the metal-phase of the same films. The deposition technique and substrate for each literature dataset are given in the legend. The thickness of all films is on the order of 100 nm. Note that, in ref. [41], the authors compared their results with ref. [42], and they are very close, so we only plotted results from ref. [41].

dominates. We are unsure about the origin of the feature around 10 μm in the metallic phase, though the wavelength corresponds to a vibrational resonance in V₂O₅^[48] that may be present in some of our films, especially on the surface. We did not find any clear Raman modes of V₂O₅ in our samples, as shown in Figure 2c, indicating that, at most, the amount of V₂O₅ is small. It is not clear why the feature disappears from our data for the insulating phase of VO₂; however, it is possible that this feature is weakly observed in reflectance and ellipsometry measurements when VO₂ is in the insulating phase, but is enhanced as the VO₂ undergoes its insulator-to-metal transition (see Section S4, Supporting Information for a back-of-the-envelope calculation that supports this hypothesis). Another possibility is that a thin surface layer of V₂O₅ is present at high temperature, but undergoes a reversible phase transition to another stoichiometry as the temperature decreases.^[49] We also note that similar features can be found in some previously published experimental results, including for VO₂ films on sapphire, silicon, silica, and zinc oxide (ZnO).^[17,50] This feature is quite apparent on Si substrates in our data, but is much less noticeable for the film on sapphire (Figure 2g).

Despite these differences, the overall features of the refractive index for both insulating and metallic phases are quite consistent between all of our films. In particular, the refractive-index values are very similar between all of the films in the insulating phase in the mid-infrared region from 2 to 11 μm, which is also the region of the lowest optical losses. This is in stark contrast to electrical measurements using macroscopically spaced electrodes that are dramatically different between the films (Figure 2b): Film 1 shows a resistance change of ≈2 orders of magnitude across the IMT; Film 2 shows ≈3 orders; Film 3 shows ≈4 orders; and in Film 4, no change could be observed at all, likely due to the small-scale cracks in the film. In general, such significant differences in electrical properties are likely due to variations in the defects, grain sizes, continuity at grain boundaries, surface roughness, etc., each of which may partially influence the macroscopic current path in the films, since distance between the electrodes is

on the order of several millimeters. However, such structural features are much smaller than the scale of the optical wavelength, and therefore their impact on the optical properties is expected to be relatively minor, especially at the longer wavelengths.

For a more-comprehensive comparison, we plot the complex refractive index of Film 1, together with data from a selection of the literature,^[7,18,19,22,41–44] in Figure 3. Most existing characterization works focus on the visible and near-infrared region, in which the optical properties of VO₂ differ substantially, as discussed previously. In the mid-infrared region, there are much fewer such measurements. The data from ref. [41] (from 1996) differ substantially from our results, and does not seem consistent with other literature data from λ ≈ 2 to 7 μm. Our data agrees well with ref. [43], though in that work the fitting process may not have fully accounted for the long-wavelength vibrational resonances of VO₂. Our data also agrees reasonably with the very recent ref. [22], which covers wavelengths up to 15 μm, though the metal-phase VO₂ from this work appears to be less metallic compared to our films.

In Figures 2 and 3, we presented refractive-index data for the insulating and metallic phases. In principle, similar measurements can be performed for any temperature throughout the IMT. However, this can be challenging because these measurements require very stable temperature control due to the hysteretic nature of the IMT and the relatively slow ellipsometric measurements. Nevertheless, intermediate-state refractive-index data is often needed for the modeling of optical and optoelectronic devices that use the gradually tunable optical properties of VO₂ (e.g., ref. [17]). It has been demonstrated that effective-medium theories (EMTs) such as the Bruggeman formalism^[51] and the Looyenga mixing rule^[16,52] can be used to approximate the refractive indices of VO₂ films within the IMT, when insulating and metallic domains coexist. Here, we use the simpler Looyenga rule

$$\tilde{\epsilon}_{\text{eff}}^s = (1 - f) \tilde{\epsilon}_i^s + f \tilde{\epsilon}_m^s \quad (1)$$

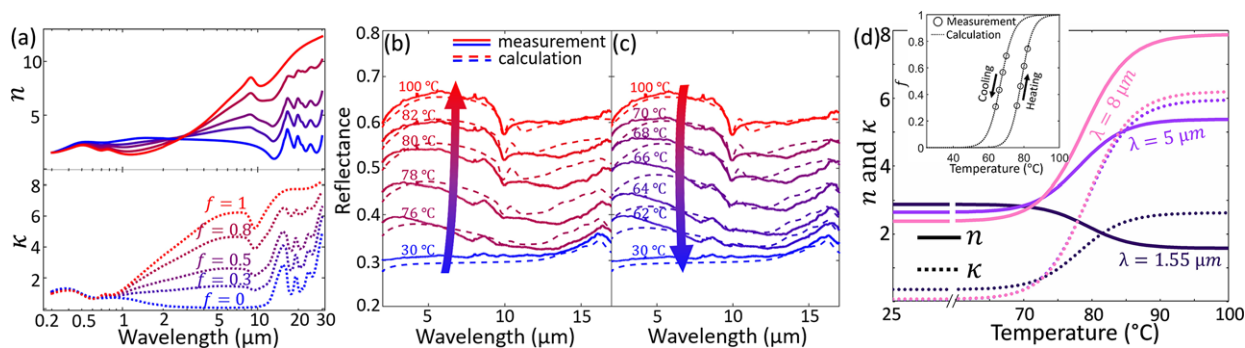


Figure 4. a) The complex refractive index of VO_2 throughout its IMT, estimated using the Looyenga effective-medium theory (EMT) and the ellipsometry fits for Film 1. The values were calculated for volume fractions of the metallic phase $f = 0, 0.3, 0.5, 0.8$, and 1, which correspond to increasing temperatures. Experimental (solid lines) and calculated (dashed lines) reflectance of Film 1 during b) heating and c) cooling, with a ramping rate of 1°C min^{-1} . d) Temperature-dependent refractive indices of Film 1 at $\lambda = 1.55, 5$, and $8 \mu\text{m}$. The inset is the extracted temperature-dependent f for a cycle of heating and cooling for Film 1.

Table 2. List of W and T_{half} values.

	Film 1	Film 2	Film 3	Film 4
W (heating) [eV]	3.37	3.57	4.85	9.60
W (cooling) [eV]	2.75	3.79	4.15	7.14
T_{half} (heating) [$^\circ\text{C}$]	78.5	78.1	75.1	72.1
T_{half} (cooling) [$^\circ\text{C}$]	67.1	66.0	72.2	65.7

In Equation (1), $\tilde{\epsilon} = \tilde{n}^2 = (n + i\kappa)^2$ is the complex dielectric function of VO_2 , f is the temperature-dependent volume fraction of the metal-phase VO_2 domains within the film, and s varies from -1 to 1 depending on the shape of the metallic inclusions. We used the empirical value of $s = 1/3$ for thin-film VO_2 .^[16] The effective refractive index is plotted in **Figure 4a** for different values of f , given the complex-refractive-index data for Film 1.

The phase co-existence can be understood as a first-order equilibrium, and therefore the temperature dependence of f can be expressed as^[16,51]

$$f(T) = \frac{1}{1 + \exp\left[\frac{W}{k_B} \left(\frac{1}{T} - \frac{1}{T_{\text{half}}}\right)\right]} \quad (2)$$

where W contains information about the width of temperature range of the IMT and T_{half} is the temperature at which half of the volume of the film is in the metallic state. Note that due to the hysteresis in VO_2 , the value of T_{half} is different for heating and cooling (in fact, there may be an infinite number of values of T_{half} , if minor loops within the hysteretic region of VO_2 are considered^[53]).

For a given W and T_{half} , Equations (1) and (2) can be used to calculate the temperature-dependent $\tilde{n}(T)$, which can then be used for optics calculations. To determine W and T_{half} during the heating and cooling stages, we fit a calculation of the normal-incidence temperature-dependent reflectance in the mid infrared to our FTIR measurements, taken at temperature steps of 2°C . The best-fit values for Films 1–4 are listed in **Table 2** and we chose Film 1 as a representative to show the agreement with the exper-

iments (Figure 4b,c; for Films 2–4, see Section S5, Supporting Information).

Once $f(T)$ is determined (e.g., the inset of Figure 4d), one can obtain the complex refractive index at any wavelength of interest across the IMT, as shown in Figure 4d where we picked three free-space wavelengths ($1.55, 5$, and $8 \mu\text{m}$) to show the evolution of n and κ with increasing temperature.

4. Conclusion

Using a combination of variable-angle spectroscopic ellipsometry (VASE), temperature-dependent reflectance measurements, and effective-medium theory (EMT), we extracted temperature-dependent complex-refractive-index values for thin films of vanadium dioxide (VO_2) over the wavelength range from 300 nm to $30 \mu\text{m}$. We compared the results for VO_2 films of different thicknesses, on different substrates, and grown using different synthesis methods. We found that there were very large differences in electrical properties and optical properties at wavelengths below $2 \mu\text{m}$ among the films, but relative consistency in the mid and far infrared, especially in the $2\text{--}11 \mu\text{m}$ region, which also corresponds to low optical losses for the insulating phase. Our full datasets, provided in the Supporting Information, will be useful for those seeking to perform simulations of optical and optoelectronic devices based on VO_2 .

Supporting Information

Supporting Information is available from the Wiley Online Library or from the author.

Acknowledgements

The authors acknowledge support from the Office of Naval Research (MK: N00014-16-1-2556, SR: N00014-16-1-2398), the National Science Foundation (MMQ: DMR-1255156 and IIP-1827536), and the Deutsche Forschungsgemeinschaft (CR: RO1198/21-1). Some of the fabrication and experiments were performed at the Materials Science Center (MSC) and the Soft Materials Laboratory (SML), both shared facilities managed by College of Engineering at the University of Wisconsin–Madison.

Conflict of Interest

The authors declare no conflict of interest.

Keywords

ellipsometry, insulator-to-metal transition, optical thin films, vanadium dioxide

Received: May 7, 2019

Published online:

- [1] J. Nag, R. F. Haglund, E. A. Payzant, K. L. More, *J. Appl. Phys.* **2012**, 112, 103532.
- [2] B. Wu, A. Zimmers, H. Aubin, R. Ghosh, Y. Liu, R. Lopez, *Phys. Rev. B* **2011**, 84, 241410.
- [3] D. Lei, K. Appavoo, F. Ligmajer, Y. Sonnefraud, R. F. Haglund, Jr., S. A. Maier, *ACS Photonics* **2015**, 2, 1306.
- [4] N. B. Aetukuri, A. X. Gray, M. Drouard, M. Cossale, L. Gao, A. H. Reid, R. Kukreja, H. Ohldag, C. A. Jenkins, E. Arenholz, K. P. Roche, H. A. Dürr, M. G. Samant, S. S. P. Parkin, *Nat. Phys.* **2013**, 9, 661.
- [5] C. Weber, D. D. O'Regan, N. D. M. Hine, M. C. Payne, G. Kotliar, P. B. Littlewood, *Phys. Rev. Lett.* **2012**, 108, 256402.
- [6] Z. Yang, C. Ko, S. Ramanathan, *Annu. Rev. Mater. Res.* **2011**, 41, 337.
- [7] H. Kakiuchida, P. Jin, S. Nakao, M. Tazawa, *Jpn. J. Appl. Phys.* **2007**, 46, L113.
- [8] J.-F. Xu, R. Czerw, S. Webster, D. L. Carroll, J. Ballato, R. Nesper, *Appl. Phys. Lett.* **2002**, 81, 1711.
- [9] W. Wang, Y. Luo, D. Zhang, F. Luo, *Appl. Opt.* **2006**, 45, 3378.
- [10] C. Wan, E. H. Horak, J. King, J. Salman, Z. Zhang, Y. Zhou, P. Roney, B. Gundlach, S. Ramanathan, R. H. Goldsmith, M. A. Kats, *ACS Photonics* **2018**, 5, 2688.
- [11] M. Soltani, M. Chaker, E. Haddad, R. V. Kruzelecky, D. Nikanpour, *J. Vac. Sci. Technol., A* **2004**, 22, 859.
- [12] F. Ligmajer, L. Kejik, U. Tiwari, M. Qiu, J. Nag, M. Konecny, T. Sikola, W. Jin, R. F. Haglund, Jr., K. Appavoo, D. Lei, *ACS Photonics* **2018**, 5, 2561.
- [13] M. A. Kats, R. Blanchard, S. Zhang, P. Genevet, C. Ko, S. Ramanathan, F. Capasso, *Phys. Rev. X* **2013**, 3, 041004.
- [14] J. Jian, A. Chen, Y. Chen, X. Zhang, H. Wang, *Appl. Phys. Lett.* **2017**, 111, 153102.
- [15] Y. Zhao, J. Hwan Lee, Y. Zhu, M. Nazari, C. Chen, H. Wang, A. Bernussi, M. Holtz, Z. Fan, *J. Appl. Phys.* **2012**, 111, 053533.
- [16] J. Rensberg, S. Zhang, Y. Zhou, A. S. McLeod, C. Schwarz, M. Goldflam, M. Liu, J. Kerbusch, R. Nawrodt, S. Ramanathan, D. N. Basov, F. Capasso, C. Ronning, M. A. Kats, *Nano Lett.* **2016**, 16, 1050.
- [17] J. Rensberg, Y. Zhou, S. Richter, C. Wan, S. Zhang, P. Schöppe, R. Schmidt-Grund, S. Ramanathan, F. Capasso, M. A. Kats, C. Ronning, *Phys. Rev. Appl.* **2017**, 8, 014009.
- [18] J. Sun, G. K. Pribil, *Appl. Surf. Sci.* **2017**, 421, 819.
- [19] M. Currie, M. A. Mastro, V. D. Wheeler, *Opt. Mater. Express* **2017**, 7, 1697.
- [20] T. J. Huffman, P. Xu, A. J. Hollingshad, M. M. Qazilbash, L. Wang, R. A. Lukaszew, S. Kittiwatanakul, J. Lu, S. A. Wolf, *Phys. Rev. B* **2015**, 91, 1.
- [21] J. B. Kana Kana, J. M. Ndjaka, G. Vignaud, A. Gibaud, M. Maaza, *Opt. Commun.* **2011**, 284, 807.
- [22] J. A. Ramirez-Rincon, C. L. Gomez-Heredia, A. Corvisier, J. Ordóñez-Miranda, T. Girardeau, F. Paumier, C. Champeaux, F. Dumas-Bouchiat, Y. Ezzahri, K. Joulain, O. Ares, J. J. Alvarado-Gil, *J. Appl. Phys.* **2018**, 124, 195102.
- [23] J. A. Woollam, B. D. Johs, C. M. Herzinger, J. N. Hilfiker, R. A. Synowicki, C. L. Bungay, *Proc. SPIE* **1999**, 10294, 1029402, <https://doi.org/10.1117/12.351660>.
- [24] V. Théry, A. Boule, A. Crunteanu, J. C. Orlianges, *Appl. Phys. Lett.* **2017**, 111, 251902.
- [25] K. Nagashima, T. Yanagida, H. Tanaka, T. Kawai, *Phys. Rev. B* **2006**, 74, 172106.
- [26] D. Ruzmetov, K. T. Zawilski, V. Narayanamurti, S. Ramanathan, *J. Appl. Phys.* **2007**, 102, 113715.
- [27] J. Nag, R. F. Haglund Jr., *J. Phys.: Condens. Matter* **2008**, 20, 264016.
- [28] T. Hanlon, R. Walker, J. Coath, M. Richardson, *Thin Solid Films* **2002**, 405, 234.
- [29] G. Rampelberg, M. Schaeckers, K. Martens, Q. Xie, D. Deduytsche, B. De Schutter, N. Blasco, J. Kittl, C. Detavernier, *Appl. Phys. Lett.* **2011**, 98, 162902.
- [30] R. Binions, G. Hyett, C. Piccirillo, I. P. Parkin, *J. Mater. Chem.* **2007**, 17, 4652.
- [31] D. H. Kim, H. S. Kwok, *Appl. Phys. Lett.* **1994**, 65, 3188.
- [32] C. Zhang, Q. Yang, C. Koughia, F. Ye, M. Sanayei, S. Wen, S. Kasap, *Thin Solid Films* **2016**, 620, 64.
- [33] H. Arwin, D. E. Aspnes, *Thin Solid Films* **1984**, 113, 101.
- [34] J. N. Hilfiker, M. Stadermann, J. Sun, T. Tiwald, J. S. Hale, P. E. Miller, C. Aracne-Ruddle, *Appl. Surf. Sci.* **2017**, 421, 508.
- [35] C. M. Herzinger, B. Johs, W. A. McGahan, J. A. Woollam, W. Paulson, *J. Appl. Phys.* **1998**, 83, 3323.
- [36] K. Okimura, J. Sakai, *Jpn. J. Appl. Phys.* **2009**, 48, 045504.
- [37] D. Kucharczyk, T. Niklewski, *J. Appl. Crystallogr.* **1979**, 12, 370.
- [38] F. Wooten, S. P. Davis, *Am. J. Phys.* **1973**, 41, 123.
- [39] T. E. Tiwald, D. W. Thompson, J. A. Woollam, W. Paulson, R. Hance, *Thin Solid Films* **1998**, 313–314, 661.
- [40] V. Eyert, *Annal. Phys.* **2002**, 11, 650.
- [41] H. S. Choi, J. S. Ahn, J. H. Jung, T. W. Noh, D. H. Kim, *Phys. Rev. B* **1996**, 54, 4621.
- [42] H. W. Verleur, A. S. Barker Jr., C. N. Berglund, *Phys. Rev.* **1968**, 172, 788.
- [43] M. M. Qazilbash, M. Brehm, B.-G. Chae, P.-C. Ho, G. O. Andreev, B.-J. Kim, S. J. Yun, A. V. Balatsky, M. B. Maple, F. Keilmann, H.-T. Kim, D. N. Basov, *Science* **2007**, 318, 1750.
- [44] R. M. Briggs, I. M. Pryce, H. A. Atwater, *Opt. Express* **2010**, 18, 11192.
- [45] L. L. Fan, S. Chen, Z. L. Luo, Q. H. Liu, Y. F. Wu, L. Song, D. X. Ji, P. Wang, W. S. Chu, C. Gao, C. W. Zou, Z. Y. Wu, *Nano Lett.* **2014**, 14, 4036.
- [46] C. Kübler, H. Ehrke, R. Huber, R. Lopez, A. Halabica, R. F. Haglund, A. Leitenstorfer, *Phys. Rev. Lett.* **2007**, 99, 116401.
- [47] T. J. Huffman, P. Xu, M. M. Qazilbash, E. J. Walter, H. Krakauer, J. Wei, D. H. Cobden, H. A. Bechtel, M. C. Martin, G. L. Carr, D. N. Basov, *Phys. Rev. B* **2013**, 87, 115121.
- [48] C. V. Ramana, O. M. Hussain, B. S. Naidu, P. J. Reddy, *Thin Solid Films* **1997**, 305, 219.
- [49] R. P. Blum, H. Niehus, C. Hucho, R. Fortrie, M. V. Ganduglia-Pirovano, J. Sauer, S. Shaikhutdinov, H. J. Freund, *Phys. Rev. Lett.* **2007**, 99, 3.
- [50] F. Guinneton, L. Sauques, J. Valmalette, F. Cros, J. Gavarrri, *J. Phys. Chem. Solids* **2001**, 62, 1229.
- [51] M. M. Qazilbash, M. Brehm, G. O. Andreev, A. Frenzel, P.-C. Ho, B.-G. Chae, B.-J. Kim, S. J. Yun, H.-T. Kim, A. V. Balatsky, O. G. Shpyrko, M. B. Maple, F. Keilmann, D. N. Basov, *Phys. Rev. B* **2009**, 79, 075107.
- [52] H. Looyenga, *Physica* **1965**, 31, 401.
- [53] M. Gurvitch, S. Luryi, A. Polyakov, A. Shabalov, *J. Appl. Phys.* **2009**, 106, 104504.